Journal of Biomedical Optics

SPIEDigitalLibrary.org/jbo

# Noninvasive evaluation of electrical stimulation impacts on muscle hemodynamics via integrating diffuse optical spectroscopies with muscle stimulator

Yu Shang
Yu Lin
Brad A. Henry
Ran Cheng
Chong Huang
Li Chen
Brent J. Shelton
Karin R. Swartz
Sara S. Salles
Guoqiang Yu

SPIE

# Noninvasive evaluation of electrical stimulation impacts on muscle hemodynamics via integrating diffuse optical spectroscopies with muscle stimulator

**Yu Shang,[a] Yu Lin,[a] Brad A. Henry,[a] Ran Cheng,[a] Chong Huang,[a] Li Chen,[b] Brent J. Shelton,[b] Karin R. Swartz,[c] Sara S. Salles,[d] and Guoqiang Yu[a]**
[a]University of Kentucky, Department of Biomedical Engineering, Lexington, Kentucky 40506
[b]University of Kentucky, Department of Biostatistics, Lexington, Kentucky 40536
[c]University of Kentucky, Department of Neurosurgery, Lexington, Kentucky 40536
[d]University of Kentucky, Department of Physical Medicine and Rehabilitation, Lexington, Kentucky 40536

**Abstract.** Technologies currently available for the monitoring of electrical stimulation (ES) in promoting blood circulation and tissue oxygenation are limited. This study integrated a muscle stimulator with a diffuse correlation spectroscopy (DCS) flow-oximeter to noninvasively quantify muscle blood flow and oxygenation responses during ES. Ten healthy subjects were tested using the integrated system. The muscle stimulator delivered biphasic electrical current to right leg quadriceps muscle, and a custom-made DCS flow-oximeter was used for simultaneous measurements of muscle blood flow and oxygenation in both legs. To minimize motion artifact of muscle fibers during ES, a novel gating algorithm was developed for data acquisition at the time when the muscle was relaxed. ES at 2, 10, and 50 Hz were applied for 20 min on each subject in three days sequentially. Results demonstrate that the 20-min ES at all frequencies promoted muscle blood flow significantly. However, only the ES at 10 Hz resulted in significant and persistent increases in oxy-hemoglobin concentration during and post ES. This pilot study supports the application of the integrated system to quantify tissue hemodynamic improvements for the optimization of ES treatment in patients suffering from diseases caused by poor blood circulation and low tissue oxygenation (e.g., pressure ulcer).  [DOI: 10.1117/1.JBO.18.10.105002]

Keywords: electrical stimulation; diffuse correlation spectroscopy; muscle; blood flow; oxygenation; motion artifact; gating algorithm.

Paper 130230RR received Apr. 10, 2013; revised manuscript received Aug. 28, 2013; accepted for publication Sep. 4, 2013; published online Oct. 4, 2013.

## 1 Introduction

Pressure ulcer is a localized wound to the skin and/or underlying tissue, which affects up to 3 million adults in the United States.[1] Pressure ulcers occur when the skin and underlying tissues above the bone are compressed for a long period of time. Constant pressure against the tissue reduces blood supply to that area, which results in tissue ischemia/hypoxia and eventual necrosis.[2,3] The development of pressure ulcer can lead to several complications including sepsis, localized infection, cellulitis, osteomyelitis, pain, and depression.[4,5] Ultrasound imaging results have recently shown that early pressure ulcers may originate from deep tissues attached to the bone and spread upward, eventually to the skin.[6] Therefore, measurements of deep tissue hemodynamics may provide information for early diagnosis and therapeutic monitoring of pressure ulcers before they are apparent on the skin surface.

Conventional ulcer care and treatment include debridement, dressing, nutrition, and surgical repair,[4,7] which are labor intensive and associated with high cost as they require the cooperation and skills of an interdisciplinary health care team. As one of the adjunctive therapies for ulcer management, transcutaneous electrical stimulation (ES) is simpler and less labor intensive with lower cost compared to conventional therapies. Transcutaneous ES has been used to treat both superficial tissues and deeper structures. ES at relatively high frequency (100 to 1000 Hz) and low current intensity (<1 mA) is often used to treat ulcers in superficial tissues[8–10] via triggering electrochemical repair mechanism of cells.[11,12] The delivered electrical potentials can influence activities and functional capacities of fibroblasts, macrophages, and neutrophils,[11,13,14] thus enhancing wound healing.

Deep muscles are found to be more susceptible to the external pressure, which deprives tissue of oxygen supply.[15] More severely, injuries to muscle evolve undetectably until massive damages occur.[15] Therefore, the treatment and prevention of pressure ulcers in deep muscles are of critical importance. As mentioned earlier, tissue ischemia/hypoxia resulting from the prolonged local pressure on the tissue is the major cause that eventually leads to pressure ulcer.[2,3,16] Correspondingly, improving tissue blood flow and oxygenation in deep muscles by ES is a straightforward way for the treatment and prevention of pressure ulcers. ES at relatively low frequency (40 Hz) and high current intensity (35 mA) can be used to treat ulcers in deep tissue.[17] Although ES electrodes are placed on the surface of skin, the delivered electrical pulses can be transmitted to muscle end-plate, activating the muscle pump and eliciting muscle fiber contractions.[18,19] The contractile muscles pump arterial blood directly into capillaries,[15] thus improving both microcirculation and tissue oxygenation. ES-induced muscle activities are especially critical for patients with spinal cord or brain injury since many of them lose an awareness of the warning signals that would prompt action against the prolonged pressure.[7]

Address all correspondence to: Guoqiang Yu, University of Kentucky, Department of Biomedical Engineering, Lexington, Kentucky 40506. Tel: 859-257-9110; Fax: 859-257-1856; E-mail: guoqiang.yu@uky.edu

0091-3286/2013/$25.00 

The ulcer treatments by ES, however, have been performed empirically and ES parameters were selected randomly across a wide range.[7,11,15,20–23] Treatment outcomes were simply evaluated by visible changes of tissue mass and/or wound volume[7,11] rather than intrinsic hemodynamic changes in ulcerous tissues. The random selection of ES parameters is mainly due to the lack of quantitative technologies for instantly and continuously evaluating tissue hemodynamic improvements that are closely associated with the increased muscle activity during ES. Moreover, minimizing muscle fiber motion artifacts in hemodynamic measurements during ES is known to be a technical challenge.

Technologies currently used to evaluate blood flow improvements by ES include Doppler ultrasound[21,22] and laser Doppler flowmetry (LDF).[23] Although Doppler ultrasound can assess blood flow in large vessels, the pressure ulcer is a condition caused mainly by poor microcirculation. LDF measures microvascular blood flow only in superficial tissues, not in deep muscles. Tissue oxygen level ($PO_2$) has been measured using $O_2$ microelectrode or transcutaneous oxygen measurement ($TcPO_2$) to evaluate ES impact on muscle oxygenation.[24] However, $O_2$ electrode measurement is invasive, and $TcPO_2$ is a complicated interaction between skin, fat, and muscle. Furthermore, although previous studies have evaluated ES impacts on either tissue blood flow[21–23] or oxygenation,[24–26] none of them have measured both quantities simultaneously. Since tissue blood flow and oxygenation are usually interactive, there is a critical need to develop noninvasive techniques that can continuously monitor both blood flow and oxygenation in deep muscles during ES.

Near-infrared spectroscopy (NIRS) offers a noninvasive, fast, portable, and low-cost alternative for repetitive bedside monitoring of deep tissue oxygenation.[27–33] NIRS can probe tissue hemodynamics millimeters to centimeters below the tissue surface as tissue absorption in the NIR range (650 to 950 nm) is relatively low. The NIR absorption spectra of major tissue chromophores, particularly oxy- and deoxy-hemoglobin, differ significantly. As a result, NIRS is sensitive to the changes in hemoglobin concentration and blood oxygen saturation ($StO_2$) in tissue microvasculature. NIRS has been used to evaluate ES impact on $StO_2$ in skeletal muscles,[25,26] although it does not directly measure tissue blood flow. An emerging dynamic NIR technique, namely diffuse correlation spectroscopy (DCS), has also been developed for direct and noninvasive measurement of blood flow in various tissues,[31,34–44] including human skeletal muscles.[45–56] Similar to NIRS, DCS also utilizes NIR light to penetrate deep tissues. However, NIRS monitors tissue blood oxygenation variations through quantifying the relatively slow changes in light intensity level due to the slow changes in tissue absorption and scattering, whereas DCS monitors directly the motion of moving scatterers (mainly red blood cells) in tissue through quantifying the fast temporal fluctuations in light intensity.[47,57,58] Therefore, DCS is considered as a dynamic NIR technique as opposed to the static NIRS.[34] DCS measurements of tissue blood flow changes have been extensively validated to other standards, including power spectral Doppler ultrasound,[43] Doppler ultrasound,[35,40] LDF,[31,41] Xenon computed tomography,[39] fluorescent microsphere flow measurement,[44] and arterial-spin-labeled magnetic resonance imaging.[54] DCS has also been combined with NIRS in hybrid instruments to simultaneously measure tissue blood flow and oxygenation.[36,38,47,49,52,53]

The hybrid DCS/NIRS instruments and combined fiber-optic probes are relatively large, complex, and expensive.[31,39,47] Recently, our group has developed a portable dual-wavelength DCS flow-oximeter[46] for simultaneous measurement of variations in tissue blood flow and oxygenation. This portable device has been used to investigate hemodynamic changes in muscle,[46,48,50,51] brain,[41,42] and tumor.[37] The goal of the present study was to integrate the novel DCS flow-oximeter and a muscle electrical stimulator to noninvasively evaluate ES treatment effects and optimize ES parameters for maximizing hemodynamic improvements in deep tissues. We applied ES pulses at low, medium, or high frequency (2, 10, or 50 Hz) to generate a single twitch, multiple twitches, or fused tetanus of the quadriceps muscle. A novel gating algorithm was developed to control data acquisition at time points when muscle fiber motion was minimal. Muscle hemodynamic responses to ES were continuously monitored, and the results at different stimulation frequencies were compared for the optimization of treatment effect. In addition, local hemodynamic changes in contralateral leg muscle (without ES) as well as systemic changes (blood pressure and heart rate) were also continuously monitored to evaluate the interactions among the local muscles and the global system of whole body. To the best of our knowledge, we report in this article the first simultaneous and continuous measurement of muscle blood flow and oxygenation responses during ES.

## 2 Methods

### 2.1 *Integrated System for Hemodynamic Monitoring of Muscle Responses to ES*

Figure 1 illustrates an integrated system including a custom-made DCS flow-oximeter [Fig. 1(a)],[36,41,42,45,46,48,49,52,53] a laptop controller [Fig. 1(b)], a rectify circuit [Fig. 1(c)], and a four-channel commercial muscle stimulator [Theratouch 4.7, Rich-Mar Corp., Tennessee, Fig. 1(d)]. The DCS flow-oximeter was used to monitor muscle hemodynamic responses to ES delivered by the muscle stimulator. The biphasic pulses generated by channel #1 (CH1) of the stimulator were rectified by a custom-made circuit. The output from the circuit was read by a digital I/O line of an analog-to-digital (A/D) board (USB-6009, National Instrument Corp., Texas) to judge the status of ES "on" or "off." A gating algorithm based on the ES status was designed to control the data acquisition at time points when muscle fiber motions were minimum (i.e., ES was off). The integrated system was controlled automatically by the A/D board connected to the laptop controller via an USB port. Details for each component of this integrated system are described below.

### 2.2 *DCS Flow-Oximeter for the Monitoring of Muscle Hemodynamics*

The DCS flow-oximeter [Fig. 1(a)] consisted of two pairs of coherent laser sources at 785 and 854 nm (Crystalaser Inc., Nevada), four single-photon-counting avalanche photodiode (APD) detectors (det1 to det4, PerkinElmer Inc., Canada), and a four-channel autocorrelator board (correlator.com, New Jersey). Briefly, the two lasers were switched on (~0.7 s) and off (~0.7 s) by a transistor-transistor logic control unit, launching long-coherence NIR light alternatively into the tissue via multimode source fibers (diameter = 200 $\mu$m), and the light

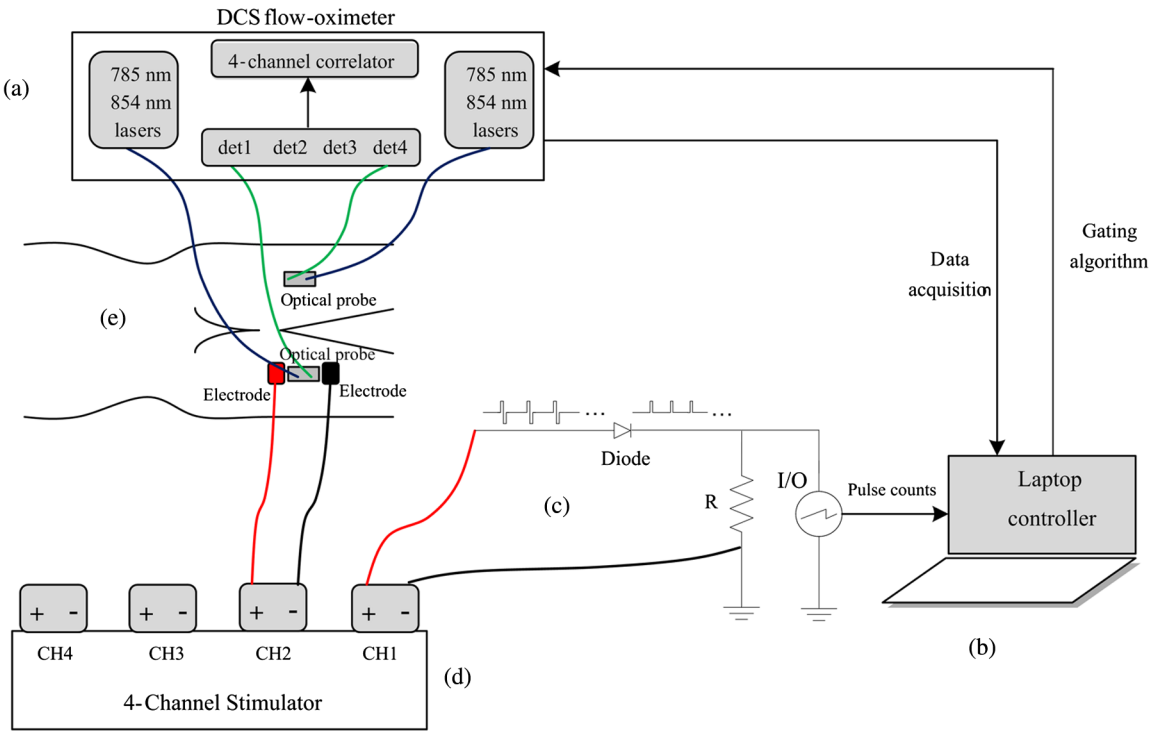


**Fig. 1** A schematic illustration of the integrated system, including a custom-made diffuse correlation spectroscopy (DCS) flow-oximeter (a), a laptop controller (b), a rectifying circuit (c), and a four-channel muscle stimulator (d). A pair of electrodes was placed on the right leg and two fiber-optic probes were taped on the two legs, respectively (e).

transported/scattered through the tissue was collected by single-mode detector fibers (diameter = 5.6 $\mu$m) connected to the APDs. The source and detector fibers were placed on the tissue surface at a distance of 2.5 cm [Fig. 1(e)]. The light intensity fluctuation with time in a single speckle area of tissue (~25 $\mu m^2$) detected by the single-mode fiber was associated with the motion of red blood cells in tissue and can be quantified by the decay of intensity autocorrelation function calculated by the autocorrelator. From the normalized intensity autocorrelation function, the electric field temporal autocorrelation function was determined, which satisfied the correlation diffusion equation in highly scattering media.[57,58] By fitting the electric field autocorrelation curve to an analytical solution of correlation diffusion equation with a semi-infinite medium geometry, a blood flow index ($\alpha D_B$) was extracted.[31,45] The semi-infinite geometry has been broadly used in NIRS/DCS data analyses for the study of skeletal muscles.[31,33,48,53,56] Here $D_B$ is the effective diffusive coefficient and $\alpha$ is the fraction of light scattering events from moving red blood cells. The goal of the curve fitting was to find the best $\alpha D_B$ that minimized the sum of squared differences between the measured and calculated autocorrelation functions. The fitting was implemented by the Nelder-Mead algorithm (fminsearch function) in MATLAB 2010b (Mathwork Inc., Massachusetts).

On the other hand, the reductions in light intensities measured at the two wavelengths (785 and 854 nm) depended on the concentrations of tissue absorbers (primarily hemoglobin in red blood cells). The changes of oxy- and deoxy-hemoglobin concentrations ($\Delta[HbO_2]$) and $\Delta[Hb]$) relative to their baseline values (determined before physiological changes) were calculated from the measured light intensity changes using modified Beer-Lambert law,[30,59,60] where the mean photon pathlength through the tissue was a product of the source-detector (S-D) distance and differential pathlength factor (DPF). In this study, the S-D distance was 2.5 cm, and DPFs were 5.56 at 785 nm and 5.17 at 854 nm, determined based on the literature.[48,60]

Two fiber-optic probes were constructed with optical fibers confined at an identical S-D separation (2.5 cm) by a black foam pad. The two probes connected to the DCS flow-oximeter [Fig. 1(a)] worked in parallel for hemodynamic measurements in quadriceps muscles of the two legs, respectively. The sampling time for a complete frame of flow and oxygenation measurements in both legs was 1.5 s.

### 2.3 *Muscle Stimulator for the Delivering of ES Pulses to Muscle*

The muscle stimulator delivered ES pulses to muscle via two electrodes [Figs. 1(d) and 1(e)]. Four channels in the stimulator worked in parallel with identical pulse outputs. In the present study, channel #2 (CH2) output was used for muscle stimulation and CH1 output for reading of muscle fiber status (contraction versus relaxation). The stimulator generated continuously cycling outputs consisting of biphasic pulses at a target frequency for 2 s (on) followed by a 2 s break (off). The current ramp up/down was set to be 1 s. Each biphasic pulse consisted of a positive phase and a negative phase with a width of 200 $\mu$s and an interval of 50 $\mu$s. The two phases had the same magnitude of current, yielding a zero net charge on muscle.

### 2.4 *Gating Control for Minimizing Muscle Motion Artifacts in Optical Measurements*

Optical measurements were gated based on ES outputs indicating no stimulation such that muscle fiber would be at resting status (relaxation) during data collection to minimize motion

artifacts. This gating algorithm is similar to that reported in our previous study.[49] Both algorithms aimed to record data at the time when the muscle is at resting status. In our previous study,[49] forearm muscle status during a handgrip exercise was judged directly from the hand position output by a dynamometer. In the present study, we built a circuit to detect the occurrence of ES pulses on the thigh muscle. As an example, the gating algorithm for ES at 2 Hz is illustrated in Fig. 2. The gating algorithms for ES at 10 and 50 Hz followed the same principle. A rectifying circuit [a silicon diode plus a 200 Ω resistor, Fig. 1(c)] was designed to cut off the negative pulses from CH1, and its output was connected to a digital I/O line of the A/D board for reading the "on" or "off" status of ES pulses. Since the outputs from all channels of the stimulator were synchronized, muscle status (contraction or relaxation) controlled by CH2 could be read from the CH1 output (on or off). A digital counter with a temporal resolution of 100 ns was set in the A/D board to detect the ES pulses generated from CH1 [Fig. 2(a)]. When ES was on, pulse counts increased continuously from the initial value of zero. Once pulse counts remained unchanged within a short period of time slightly longer than the interval of ES pulses (e.g., 500 ms at 2 Hz), ES was considered to be "off" and the counter was then reset to zero [Fig. 2(b)]. After a short period of delay (300 ms) to account for the residual motion of muscle fibers after contraction [Fig. 2(c)], the DCS flow-oximeter started to collect one frame of hemodynamic data within 1.5 s [Fig. 2(d)]. This gating algorithm enabled data recording only at time points when muscle fiber motion was minimal.

### 2.5 *Experimental Protocols*

This study was approved by the institutional review board (IRB) at the University of Kentucky. Ten healthy volunteers (six males and four females) between the ages of 21 and 42 years participated in this study with IRB approved consents. The subject was laid supine on a bed with his/her knee fully extended (180 deg knee angle). For continuous monitoring of beat-to-beat arterial blood pressure (including systolic, diastolic, and mean blood pressure) and heart rate, a noninvasive finger plethysmograph sensor (Portapres, FMS Inc., Netherlands) was attached to the middle finger of the right hand with the subject's right forearm fully extended on a padded cushion at heart level. A pair of self-adhesive foam electrodes (2 in. × 2 in. square, Rich-Mar Corp., Tennessee) was taped on top of the motor points over the middle of quadriceps muscles (rectus femoris) [Fig. 1(e)]. The electrodes were connected to CH2 of the muscle stimulator. A fiber-optic probe was taped on the skin between the two electrodes and connected to the DCS flow-oximeter for hemodynamic monitoring of muscle responses to ES. Another identical fiber-optic probe was taped on the same location of the left thigh for control measurements. Before installing the probes and electrodes, a skinfold caliper (Lange 85300, Texas) was used to measure the adipose tissue thickness (ATT) overlaying the quadriceps muscles at the locations beneath the two probes.

Prior to ES experimental protocol, each subject participated in a test to determine the maximum ES currents at three different stimulation frequencies (i.e., 2, 10, and 50 Hz). The maximum ES current was set to create largest visible muscle contractions within the pain tolerance of each subject. For the ES experiment, after a baseline measurement lasting for 3 min, the maximum biphasic electrical current was applied to the quadriceps muscle of the right leg for 20 min, followed by a recovery measurement for additional 20 min. Electrical stimulations at 2, 10, and 50 Hz with corresponding current intensities (selected based on the subject's maximal pain tolerance) were applied on each subject in three sequential days in order to avoid the interference among the multiple stimulations. On each day, the subject received ES treatment once at one single frequency (2, 10, or 50 Hz).

### 2.6 *Data Analysis*

DCS measurements at two wavelengths (785 and 854 nm) generated two blood flow curves. We have previously observed that DCS flow measurements are not sensitive to wavelength.[46] Similarly, in this study, the difference in relative blood flow (rBF) between the two wavelength measurements was <3%. Following the way in previous studies,[37,41,42,46,48,50,51] blood flow index (i.e., $\alpha D_B$) derived from one wavelength (785 nm) was used for data analysis. rBF was calculated by

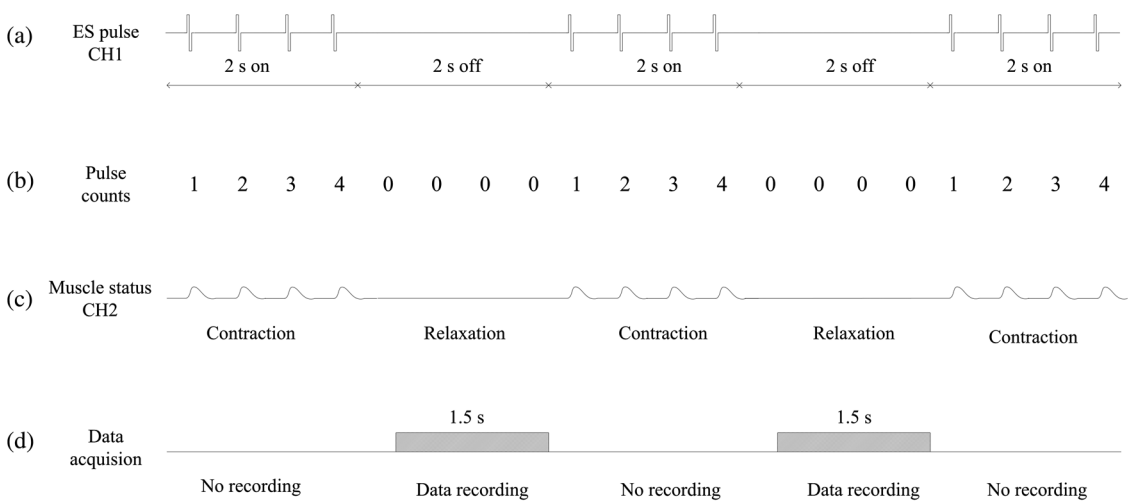


**Fig. 2** A gating algorithm for optical data acquisition during electrical stimulation (ES) at 2 Hz. The outputs from channel #1 (CH1) (a) and channel #2 (CH2) (c) of muscle stimulator were synchronized; thus the muscle status (contraction or relaxation) controlled by CH2 could be read from the CH1 output ("2 s on" or "2 s off"). A digital counter in the A/D board was used to detect the ES pulses generated from CH1. The pulse counts increased continuously when ES was on and remained unchanged when ES was off (b). Optical data were recorded within 1.5 s when the ES was off (d).

normalizing/dividing the measured $\alpha D_B$ to its 3-min average baseline value before ES. In order to quantify physiological changes (rBF, $\Delta[HbO_2]$, $\Delta[Hb]$, mean arterial blood pressure (ABP), and heart rate) throughout ES, during-ES responses were characterized as the average of data points during the last 3 min of ES, and post-ES responses were determined by averaging the data points during the last 3 min of the recovery period. The averaged responses over 10 subjects were presented as means ± standard errors (error bars) in figures.

To investigate the changes in hemodynamic parameters (rBF, $\Delta[HbO_2]$, $\Delta[Hb]$) among different time periods and whether ES frequency and muscle site affect these changes, data were first analyzed using two-way repeated measures ANOVA (RMA) with main effects of time period (pre-, during, and post-ES), muscle site (stimulation and control) and ES frequency (2, 10, and 50 Hz), and interaction effects between time period and muscle site as well as between time period and ES frequency. In the cases where interaction effects (between time period and muscle site, and/or between time period and ES frequency) were found, RMA in each specific muscle site and/or at each specific ES frequency was then conducted to investigate the main effect of time period adjusting for muscle site or ES frequency when necessary. In the cases where the main effect of time period was found, *post hoc* least significant difference (LSD) tests were then conducted for pairwise comparisons among the three time periods. If hemodynamic changes among the time periods were identified to be significant and the interaction between time period and ES frequency was significant, further analyses on these changes, using two-way RMA with muscle site and ES frequency followed by *post hoc* analysis, were conducted to evaluate how ES frequency affects these changes. If hemodynamic changes were identified to be significant on both stimulated and control muscle sites, additional analyses using two-way RMA with muscle site and ES frequency followed by *post hoc* analyses were conducted to evaluate whether these changes are different between the stimulated and control muscles. Linear regression was used to investigate the correlations among different physiological variables. $p < 0.05$ was considered significant for all statistical results. All statistical analyses were implemented by the statistics toolbox of MATLAB 2010b (Mathworks Inc., Massachusetts).

## 3 Results

All subjects completed the protocols without adverse complications. The ATTs over 10 subjects were $0.76 \pm 0.07$ and $0.74 \pm 0.06$ cm in muscles with and without ES, respectively. The ES currents applied to the subjects were $48.9 \pm 4.2$ mA at 2 Hz, $33.4 \pm 3.4$ mA at 10 Hz, and $25.7 \pm 3.3$ mA at 50 Hz, respectively. The subjects tended to tolerate less ES current intensity at higher frequency.

### 3.1 *Effect of Gating Control in Optical Measurements*

Figure 3 shows results from a preliminary test in a single subject demonstrating the effect of gating control in DCS flow measurements during 3-min ES at 2 Hz. The two trials were performed using the same ES current intensity and separated by more than 30 min. Without gating, ES-induced muscle fiber motions introduced large artifacts in DCS data, leading to substantial overestimates of rBF [Fig. 3(a)]. The gating algorithm greatly reduced noises due to motion artifacts [Fig. 3(b)].

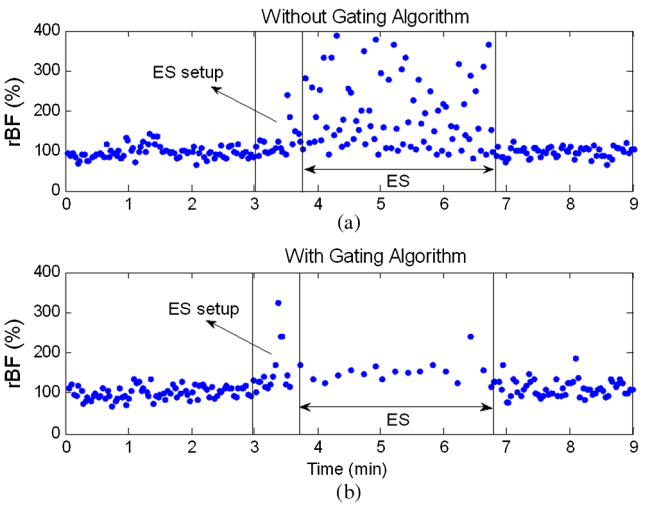


**Fig. 3** Relative blood flow (rBF) responses during 3-min ES at 2 Hz, measured by the DCS flow-oximeter without (a) or with (b) the gating algorithm. The time period between the first and second marks (vertical lines) indicates the transition to adjust the ES current from zero to the maximum tolerant level (i.e., ES setup). The optical data collected during the period of ES setup were excluded due to the large noises induced by the adjustment of ES current. The ES started from the second mark and ended at the third mark. The gating algorithm (b) significantly reduced noise due to motion artifact.

### 3.2 *Time Course Physiological Responses to ES*

Figures 4 and 5 show average time course physiological responses to ES over 10 subjects measured from stimulated (right leg) and control (left leg) muscles, respectively. Physiological variables measured included rBF, $\Delta[HbO_2]$, $\Delta[Hb]$, ABP, and heart rate. Physiological responses to ES at low (2 Hz), medium (10 Hz), and high (50 Hz) frequencies are demonstrated in (a), (b), and (c), respectively. Data obtained from 10 subjects were aligned based on the marks indicating the beginning and end of the ES (see the vertical lines in figures). For clarity of data presentation, a 1-min averaging window was applied on and shifted over the raw data for each subject. The processed datasets from 10 subjects were then averaged and displayed as mean and standard errors (error bars).

In the muscles with ES treatment (Fig. 4), rBF increased persistently during ES at all frequencies and maintained at a level higher than its baseline for 20 min post ES. There were remarkable increases in $\Delta[HbO_2]$ during and post ES at 10 Hz [Fig. 4(b)], but not at other two frequencies [2 and 50 Hz, Figs. 4(a) and 4(c)]. Changes in $\Delta[Hb]$ were not apparent during and post ES at all frequencies. ABP increased during ES and maintained higher than its baseline post ES, while heart rate varied around baseline throughout ES at all frequencies.

In the contralateral control muscles without ES (Fig. 5), rBF increased slightly and $\Delta[HbO_2]$ and $\Delta[Hb]$ varied around baseline throughout ES. However, these changes were much smaller than those observed in the stimulated muscles with ES (Fig. 4).

### 3.3 *Average Physiological Changes During and Post ES*

As described in Sec. 2.6, the mean value of data points during the last 3 min of ES or recovery period was used to quantify the physiological changes (relative to pre-ES baseline) during or

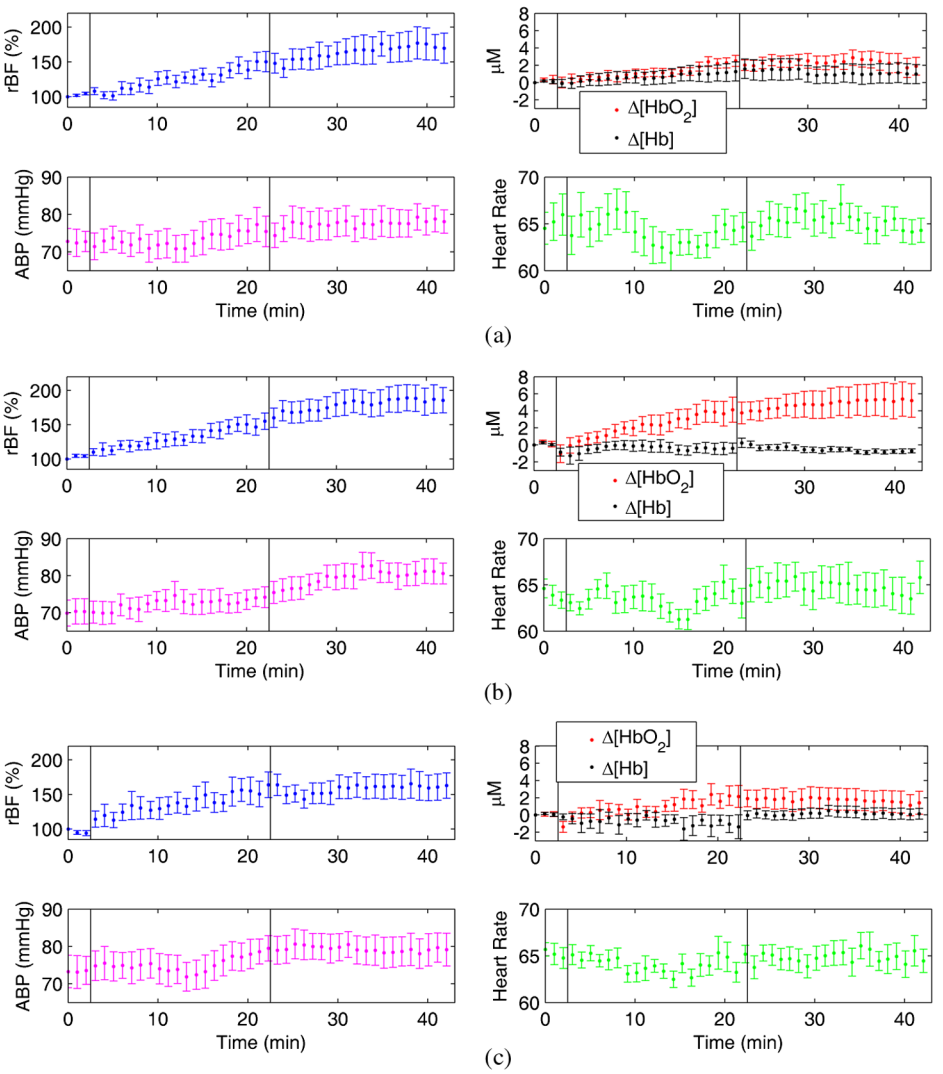


**Fig. 4** The average time course physiological responses [rBF, $\Delta[HbO_2]$, $\Delta[Hb]$, arterial blood pressure (ABP) and heart rate] to ES over 10 subjects measured from the stimulated muscles in the right legs with ES at 2 Hz (a), 10 Hz (b), and 50 Hz (c). Data obtained from 10 subjects were aligned based on the marks (vertical lines) made at the beginning and end of ES.

post ES, and results are presented in Figs. 6 and 7, respectively. Two-way RMA analyses showed that muscle site significantly affected the changes in rBF and $\Delta[Hb]$ among different time periods ($p = 0.01$ and 0.03 for rBF and $\Delta[Hb]$ respectively), leading to subsequent RMA analyses of time period adjusting for ES frequency in stimulated and control muscles, respectively. Two-way RMA analyses also showed that both muscle site and ES frequency significantly affected the changes in $\Delta[HbO_2]$ ($p = 0.002$ and 0.03 for the interactions between time period and muscle site and between time period and ES frequency, respectively), leading to subsequent RMA analyses of time period in each combination of muscle site and ES frequency.

In stimulated muscles, RMA showed that rBF differed significantly among different time periods. Compared to pre-ES baseline values, rBF increased significantly and persistently during ES [$p < 0.001$, *post hoc* LSD, Fig. 6(a)] and post ES [$p < 0.001$, *post hoc* LSD, Fig. 7(a)], with the adjustment of ES frequency effect.

Significant increases in $\Delta[HbO_2]$ (compared to pre-ES values) were also observed during ES [$p = 0.04$, *post hoc* LSD, Fig. 6(b)] and post ES [$p = 0.02$, *post hoc* LSD, Fig. 7(b)] at 10 Hz in stimulated muscles. There was also significant increase in $\Delta[HbO_2]$ during ES at 2 Hz [Fig. 6(b)], but not post ES at this stimulation frequency. Since two-way RMA analyses showed that ES frequency significantly affected $\Delta[HbO_2]$ changes among different time periods, additional analyses were performed to evaluate the effects of ES frequency on $\Delta[HbO_2]$ changes. The increases in $\Delta[HbO_2]$ at 10 Hz were significantly larger than those during ES at 50 Hz ($p = 0.04$, *post hoc* LSD) and those post ES at 2 and 50 Hz ($p = 0.03$ for both 2 and 50 Hz; *post hoc* LSD).

Taken together, ES at medium frequency (10 Hz) significantly and persistently increased both blood flow (rBF) and oxygenation ($\Delta[HbO_2]$) in stimulated muscles throughout ES (i.e., both during and post ES).

In addition, no significant differences (*post hoc* LSD) of hemodynamic changes were found in stimulated muscles between during and post ES. Linear regressions revealed that rBF changes were not significantly correlated with tissue oxygenation changes in most conditions. Exceptions included that rBF changes were correlated with $\Delta[HbO_2]$ during ES at 50 Hz ($R^2 = 0.51$, $p = 0.02$) and post ES at 2 Hz ($R^2 = 0.67$, $p = 0.004$).

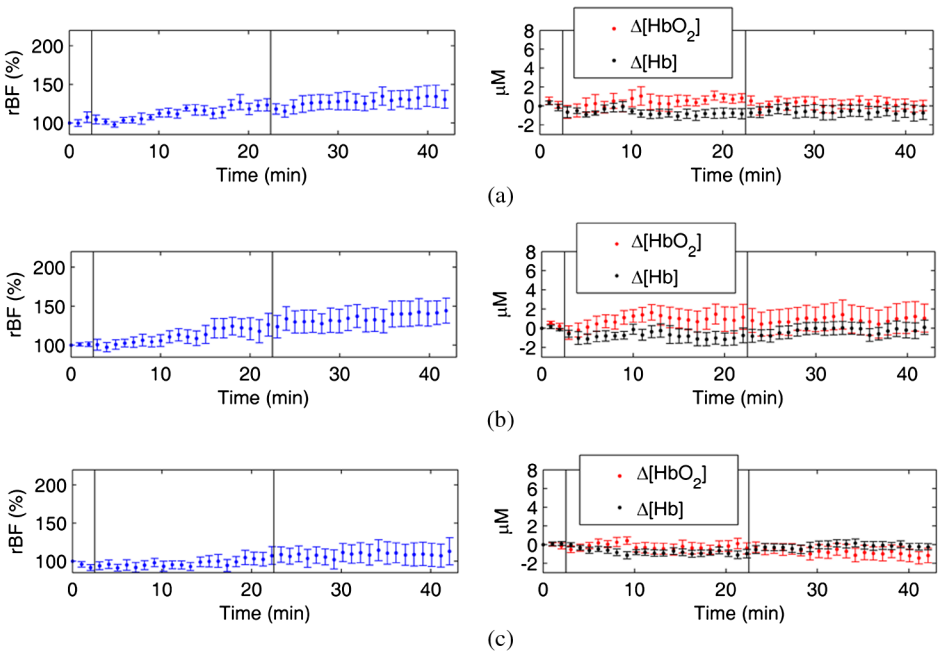


**Fig. 5** The average time course hemodynamics responses to ES over 10 subjects measured from the control muscles in the left legs without ES. The hemodynamic responses (rBF, $\Delta[HbO_2]$, $\Delta[Hb]$) to ES at low (2 Hz), medium (10 Hz), and high (50 Hz) frequencies are displayed in (a), (b), and (c), respectively. The two vertical lines (marks) indicate the beginning and end of ES.

In the contralateral (control) muscles without ES, some variables demonstrated significant changes during ES [$\Delta[Hb]$ decreased, Fig. 6(c)] or post ES [rBF increased, Fig. 7(a)]. However, additional analyses revealed that rBF increases post ES in control muscles were significantly ($p < 0.001$, *post hoc* LSD) smaller than those observed in stimulated muscles [Fig. 7(a)]. Furthermore, there were no significant increases in $\Delta[HbO_2]$ during [Fig. 6(b)] and post [Fig. 7(b)] ES in control muscles at all three frequencies.

Significant increases ($p < 0.001$) in ABP were also observed post ES [Fig. 7(d)]. The changes in heart rate were not significant [Figs. 6(e) and 7(e)]. No correlations were found among muscle hemodynamic responses, ABP, and heart rate throughout ES.

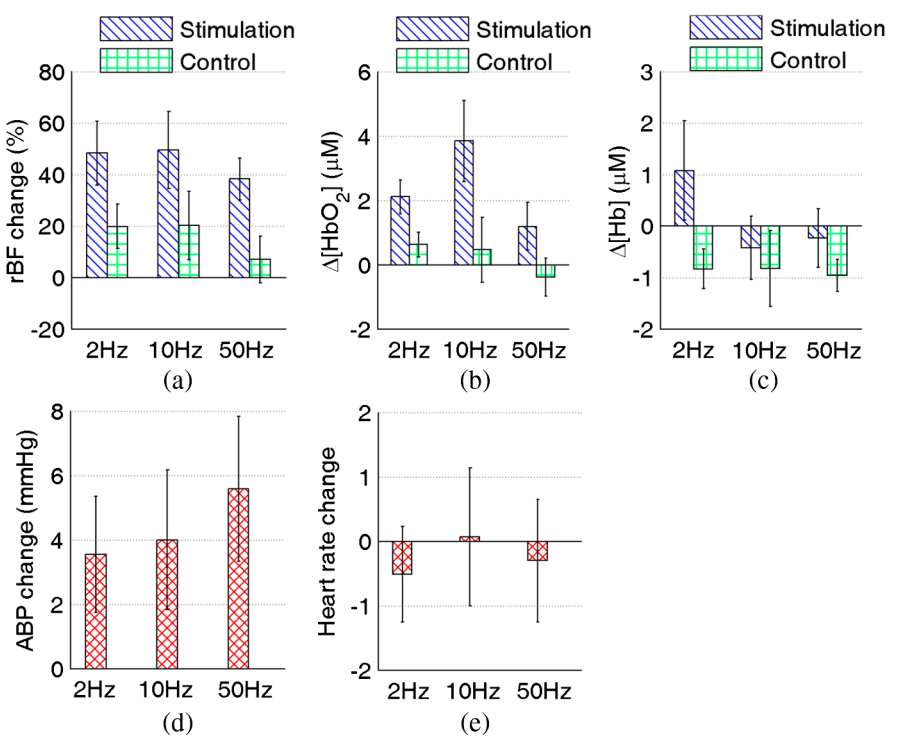


**Fig. 6** Average physiological changes (mean ± SE) over 10 subjects in rBF (a), $\Delta[HbO_2]$ (b), $\Delta[Hb]$ (c), ABP (d), and heart rate (e) during ES at 2, 10, and 50 Hz. The changes for each subject were calculated by averaging the data over the last 3 min during ES.

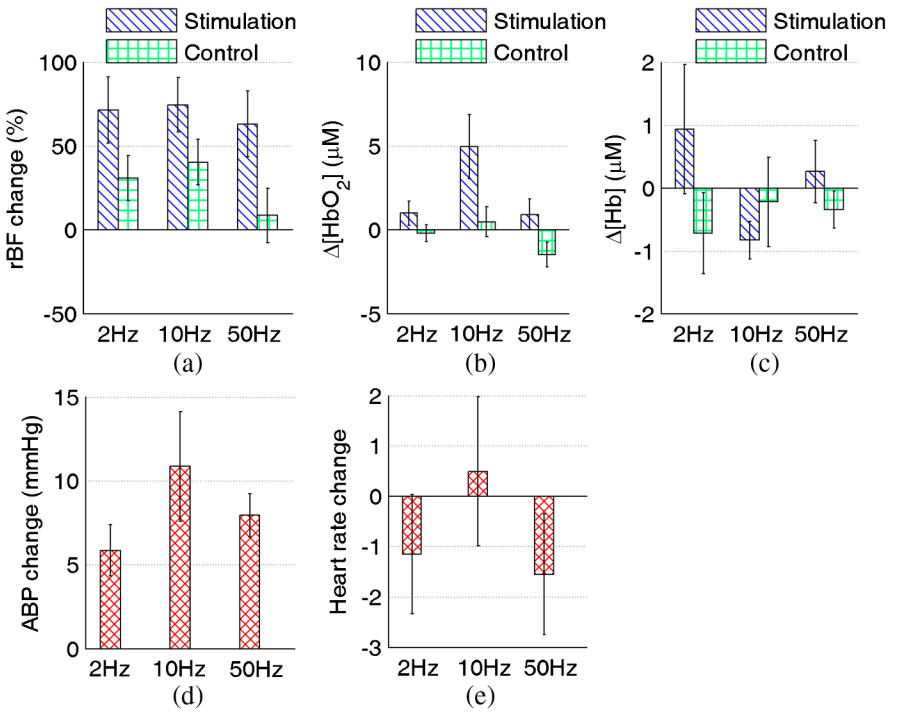


**Fig. 7** Average physiological changes (mean ± SE) over 10 subjects in rBF (a), $\Delta[HbO_2]$ (b), $\Delta[Hb]$ (c), ABP (d), and heart rate (e) after ES at 2, 10, and 50 Hz. Individual changes were calculated by averaging the physiological data over the last 3 min of the recovery period.

## 4 Discussion and Conclusions

The goal of our ES treatment is to maximize tissue hemodynamics in local muscles. Continuous measurement of muscle hemodynamics during ES provides valuable information for objectively optimizing ES effect. However, technologies available for this purpose are limited. In this study, we developed a unique integrated system (see Fig. 1) that incorporated a novel DCS flow-oximeter and a muscle stimulator for noninvasive and continuous monitoring of muscle blood flow and oxygenation responses to ES. A gating algorithm was designed to control the data collection only at time points when muscle was under relaxation (see Fig. 2), which greatly reduced noises due to muscle fiber motion during ES (see Fig. 3). We also compared tissue hemodynamic improvements generated by different types of muscle contractions. ES at relatively low frequency (2 to 40 Hz) and high current intensity (10 to 45 mA) have been previously found to be efficient in enhancing tissue blood flow for the treatment of pressure ulcers.[2,61,17] Based on those previous results, electrical stimulations at 2, 10, and 50 Hz were thus selected in the present study as representative frequencies to generate a single twitch, multiple twitches, and fused tetanus on the muscle, respectively. The current intensities (14 to 75 mA) were selected based on subjects' maximal pain tolerance.

Our ultimate goal is to use ES to treat pressure ulcers in patients with spinal cord injury (SCI). However, this pilot study aimed to adapt our novel optical techniques for evaluating ES treatment effects and to optimize ES parameters for maximizing hemodynamic improvements in deep tissues. Healthy subjects were recruited for this study because they have the ability to sense pain, which allowed us to determine their maximal tolerance to ES currents. Moreover, the use of healthy subjects for repeated testing permitted us to optimize our techniques and ES protocols. It is not practical to optimize our techniques and ES parameters using patients with SCI due to their poor mobility and loss of pain sensation. Although patients with SCI may have partial or complete impairments in their central nervous system function that controls muscle contractions, externally applied ES pulses can still stimulate their muscle pump activity by triggering the cross-bridge cycling between actin and myosin.[19] Consequently, ES-induced blood flow increases in patients with SCI have been observed to be similar to those in healthy subjects.[19,62] Therefore, the knowledge gained from the present study with healthy subjects is expected to be beneficial for future studies using SCI patients with pressure ulcers.

For future translation of the developed ES protocols to SCI patients with pressure ulcers, we may gradually increase the ES current intensity to the point of visible muscle contractions (for those without pain sensation) or maximal pain tolerance (for those with pain sensation). In addition, muscle contraction can be evaluated by detecting the electrically evoked force,[63] which may be an alternative standard for selecting ES current intensity.

Experimental results from this study demonstrate that the short-term (~20 min) ES can significantly increase muscle rBF during ES (see Figs. 4 and 6) and maintain a higher level than its pre-ES baseline for at least 20 min post ES (see Figs. 4 and 7), regardless of the applied stimulation frequencies. Previous studies also found significant blood flow increases in quadriceps muscle[21,22] or skin[23] when applying ES at medium (10 Hz)[22] or high (30 Hz)[21,23] frequency. In those studies, muscle or skin blood flow was measured by Doppler ultrasound[21,22] or LDF.[23] Although ES-induced increases in rBF had led to some improvements in tissue oxygenation (i.e., increases in $\Delta[HbO_2]$ and decreases in $\Delta[Hb]$, see Figs. 4 to 7) during or post ES at some ES frequencies, only ES at medium frequency (10 Hz) improved $\Delta[HbO_2]$ significantly and persistently during and post ES (see Figs. 6(b)

and 7(b)). Maintenance of elevated rBF or tissue oxygenation post ES has also been reported in other studies,[15,23,64] and it was attributed to the reactive hyperemia induced by ES.[15]

The level of tissue blood oxygenation reflects the balance between oxygen supply (blood flow) and oxygen consumption. These three parameters (i.e., blood flow, blood oxygenation, tissue oxygen consumption) may or may not be coupled, depending on physiological manipulations/procedures. Tissue oxygen consumption may substantially affect the coupling between the blood flow and blood oxygenation levels. For example, a high intensity foot pedal plantar flexion exercise can lead to the increases in blood flow and oxygen consumption as well as a decrease in tissue blood oxygen saturation in calf muscles due to the high tissue oxygen consumption induced by the exercise.[47,65] In the present study, ES at 10 Hz generated effectively multiple twitches of muscle fibers, which may lead to large variations in tissue oxygen consumption affecting the coupling of blood flow and tissue oxygenation. This could be the reason of why no significant correlation existed between the rBF and $\Delta[HbO_2]$ when using ES at 10 Hz. The poorly coupled hemodynamic responses further emphasize the need for simultaneous measurements of both blood flow and oxygenation changes. Previous studies have also reported either poorly coupled[47,48,65,66] or well-correlated[39] changes between the blood flow and tissue oxygenation in response to different physiological manipulations.

A single ES pulse can generate a cycle of muscle fiber twitch including a fast contraction (30 to 50 ms) and a relatively slow relaxation (100 to 300 ms).[67–69] When the interval of ES pulses (e.g., 500 ms at 2 Hz) is larger than a twitch cycle (<350 ms), different twitches are isolated and muscle fibers present the feature of a single twitch.[67,70] When the pulse interval (e.g., 100 ms at 10 Hz) is smaller than a twitch cycle (<350 ms) but larger than a contraction time (<50 ms), twitches are accumulated during the period of relaxation and muscle fibers present the feature of multiple twitches.[67,70] When the pulse interval (e.g., 20 ms at 50 Hz) is smaller than a contraction time (<50 ms), twitches are accumulated throughout the ES time and muscle fibers present the feature of fused tetanus.[67,69,70]

The multiple twitches of muscle fibers generated by ES at 10 Hz repeatedly pump arterial blood into tissue, thus constantly elevating oxygen level. Although the single twitch generated by ES at 2 Hz also improves muscle perfusion in intermittent pattern, the transient oxygen increment from single muscle contraction may be rapidly balanced by tissue oxygen consumption. Thus, limited muscle fiber twitches generated by ES at low frequency (2 Hz) are likely not sufficient to generate sustained elevation of tissue oxygen levels. ES at 50 Hz recruits bulk muscle fibers to contraction and generates large contractile force, but the fused tetanus pattern restricts the release of muscle contraction. Therefore, ES at high frequency (50 Hz) actually generates a single and longer-term contraction of bulk muscle fibers in pumping blood to tissue, which is functionally similar to ES at low frequency (2 Hz). Taken together, it is not surprising that ES at 10 Hz promotes muscle oxygen level efficiently.

ES also causes significant increases in local rBF of contralateral control leg muscles for some frequencies [see Figs. 6(a) and 7(a)] and in global ABP [see Fig. 7(d)]. These changes are likely due to systemic influences of ES on the whole body. Such systemic influences were previously found in other studies[25,64] and were attributed primarily to the increase in sympathetic nerve activity due to ES.[20,25] The sympathetic nerve activity regulates ABP as well as the release of neurotransmitters that control the muscle vessel vasodilation and vasoconstriction.[20,25] Nevertheless, hemodynamic changes in control muscles without ES were found to be significantly lower than those in stimulated muscles with ES (see Figs. 4 to 7), and no correlations were observed among muscle hemodynamic responses, ABP, and heart rate throughout ES. These findings suggest that hemodynamic improvements in stimulated muscles with ES are mainly due to the local muscle contraction rather than the systemic impact.

One concern for this study is that the DCS flow-oximeter for deep muscle measurements may be influenced by the overlaying skin and adipose tissues. It is known that the penetration depth of NIR light in biological tissues is approximately half of the S-D separation.[71] The probing depth of ~1.3 cm with the S-D separation of 2.5 cm used in the present study is much larger than the ATTs ($0.76 \pm 0.07$ and $0.74 \pm 0.06$ cm on top of the stimulated and control muscles, respectively), thus allowing for the detection of deep muscle hemodynamics. Nevertheless, future study will use optical probes with multiple S-D separations to detect hemodynamic responses in different tissue layers (i.e., skin, adipose tissue, and muscle) and correct the influence of overlying tissues on top of the muscle.

Another concern is the laser wavelengths used in DCS flow-oximeter. The laser at 785 nm is not ideal for tissue oxygenation measurement as the extinction coefficients of oxy- and deoxy-hemoglobin at this wavelength are not greatly different. Selection of the two wavelengths was restricted by the commercial availability of long-coherence lasers (>5 m) for concurrent DCS blood flow measurements. In a previous study, we have validated a dual-wavelength (785 and 854 nm) DCS flow-oximeter for tissue oxygenation measurements against a commercial tissue oximeter (Imagent, ISS Inc., Illinois); the oxy- and deoxy-hemoglobin concentration changes measured by the two devices were found to be highly correlated.[46] Furthermore, this dual-wavelength DCS flow-oximeter has been broadly used in the study of skeletal muscle,[46,48,50,51] brain,[41,42] and tumor.[37] Nevertheless, optimization of wavelengths will be the subject of our future work.

In conclusion, we have integrated the novel DCS flow-oximeter with a muscle stimulator to noninvasively and continuously monitor muscle hemodynamic improvements during and post ES at low (2 Hz), medium (10 Hz), and high (50 Hz) frequencies. Muscle fiber motion artifacts in optical measurements during ES were mitigated using a novel gating algorithm. Multiple physiological parameters, including blood flow and oxygenation in local leg muscles with or without ES, blood pressure, and heart rate, were concurrently measured during ES for the first time. Multiparameter measurements provide deeper insight into tissue physiology and allow us to investigate the complex relations of local (muscle) and systemic (blood pressure and heart rate) responses to ES. We found that multiple twitches of muscle fibers generated by ES at medium frequency (10 Hz) significantly and persistently increased both muscle blood flow and oxygenation throughout ES. Importantly, none of the 10 participated subjects experienced any discomfort during this ES intervention. This study supports the application of the integrated system to quantify muscle hemodynamic improvements for the optimization of ES treatment and holds potential for improving treatment evaluation for patients suffering from diseases caused by poor blood circulation and low tissue oxygenation (e.g., pressure ulcer).

## Acknowledgments

Research reported in this publication was supported by the National Institute of Arthritis and Musculoskeletal and Skin Diseases, part of the National Institutes of Health (NIH), under Award Number R21 AR062356 (G.Y.). The content is solely the responsibility of the authors and does not necessarily represent the official views of the NIH.

## References

1. C. H. Lyder, "Pressure ulcer prevention and management," *J. Am. Med. Assoc.* **289**(2), 223–226 (2003).
2. L. Q. Liu et al., "Pressure changes under the ischial tuberosities of seated individuals during sacral nerve root stimulation," *J. Rehabil. Res. Dev.* **43**(2), 209–217 (2006).
3. J. Leachtenauer et al., "A noncontact imaging-based approach to detecting stage I pressure ulcers," in *Ann. Int. Conf. of the IEEE Engineering in Medicine and Biology Society*, pp. 6380–6383, IEEE, New York, NY (2006).
4. H Brem and C. Lyder, "Protocol for the successful treatment of pressure ulcers," *Am. J. Surg.* **188**(1A), 9S–17S (2004).
5. L. R. Pender and S. K. Frazier, "The relationship between dermal pressure ulcers, oxygenation and perfusion in mechanically ventilated patients," *Intensive Crit. Care Nurs.* **21**(1), 29–38 (2005).
6. N. Kanno et al., "Low-echoic lesions underneath the skin in subjects with spinal-cord injury," *Spinal Cord* **47**(3), 225–229 (2009).
7. T. Janssen, C. Smit, and M. Hopman, *Prevention and Treatment of Pressure Ulcers Using Electrical Stimulati*, Springer, Berlin (2005).
8. L. C. Kloth and J. A. Feedar, "Acceleration of wound-healing with high-voltage, monophasic, pulsed current," *Phys. Ther.* **68**(4), 503–508 (1988).
9. P. E. Houghton et al., "Effect of electrical stimulation on chronic leg ulcer size and appearance," *Phys. Ther.* **83**(1), 17–28 (2003).
10. A. Jankovic and I. Binic, "Frequency rhythmic electrical modulation system in the treatment of chronic painful leg ulcers," *Arch. Dermatol. Res.* **300**(7), 377–383 (2008).
11. J. A. Feedar, L. C. Kloth, and G. D. Gentzkow, "Chronic dermal ulcer healing enhanced with monophasic pulsed electrical-stimulation," *Phys. Ther.* **71**(9), 639–649 (1991).
12. J. C. Ojingwa and R. R. Isseroff, "Electrical stimulation of wound healing," *J. Invest. Dermatol.* **121**(1), 1–12 (2003).
13. I. Taskan et al., "A comparative study of the effect of ultrasound and electrostimulation on wound healing in rats," *Plast. Reconstr. Surg.* **100**(4), 966–972 (1997).
14. M. Junger et al., "Local therapy and treatment costs of chronic, venous leg ulcers with electrical stimulation (Dermapulse (R)): a prospective, placebo controlled, double blind trial," *Wound Repair Regen.* **16**(4), 480–487 (2008).
15. L. R. Solis et al."Prevention of pressure-induced deep tissue injury using intermittent electrical stimulation," *J. Appl. Physiol.* **102**(5), 1992–2001 (2007).
16. A. R. Mawson et al., "Risk-factors for early occurring pressure ulcers following spinal-cord injury," *Am. J. Phys. Med. Rehabil.* **67**(3), 123–127 (1988).
17. A. Jercinovic and R. Karba, "Low frequency pulsed current and pressure ulcer healing," *IEEE Trans. Rehabil. Eng.* **2**(4), 225–233 (1994).
18. P. D. Faghri, J. J. Votto, and C. F. Hovorka, "Venous hemodynamics of the lower extremities in response to electrical stimulation," *Arch. Phys. Med. Rehabil.* **79**(7), 842–848 (1998).
19. P. D. Faghri and J. Yount, "Electrically induced and voluntary activation of physiologic muscle pump: a comparison between spinal cord-injured and able-bodied individuals," *Clin. Rehabil.* **16**(8), 878–885 (2002).
20. J. Petrofsky et al., "The interrelationships between electrical stimulation, the environment surrounding the vascular endothelial cells of the skin, and the role of nitric oxide in mediating the blood flow response to electrical stimulation," *Med. Sci. Monitor* **13**(9), CR391–CR397 (2007).
21. J. L. Olive et al., "Blood flow and muscle fatigue in SCI individuals during electrical stimulation," *J. Appl. Physiol.* **94**(2), 701–708 (2003).
22. P. Dobsak et al., "Low-frequency electrical stimulation increases muscle strength and improves blood supply in patients with chronic heart failure," *Circ. J.* **70**(1), 75–82 (2006).
23. A. M. Al Malty and J. Petrofsky, "The effect of electrical stimulation on a normal skin blood flow in active young and older adults," *Med. Sci. Monitor* **13**(4), Cr147–Cr155 (2007).
24. B. F. Jordan et al., "Contribution of oxygenation to BOLD contrast in exercising muscle," *Magn. Reson. Med.* **52**(2), 391–396 (2004).
25. V. Gerovasili et al., "Short-term systemic effect of electrical muscle stimulation in critically III patients," *Chest* **136**(5), 1249–1256 (2009).
26. R. M. Crameri et al., "Effect of load during electrical stimulation training in spinal cord injury," *Muscle Nerve* **29**(1), 104–111 (2004).
27. S. Fantini et al., "Non-invasive optical monitoring of the newborn piglet brain using continuous-wave and frequency-domain spectroscopy," *Phys. Med. Biol.* **44**(6), 1543–1563 (1999).
28. F. H. Tian, B. Chance, and H. L. Liu, "Investigation of the prefrontal cortex in response to duration-variable anagram tasks using functional near-infrared spectroscopy," *J. Biomed. Opt.* **14**(5), 054016 (2009).
29. M. A. Franceschini et al., "Diffuse optical imaging of the whole head," *J. Biomed. Opt.* **11**(5), 054007 (2006).
30. G. Strangman, M. A. Franceschini, and D. A. Boas, "Factors affecting the accuracy of near-infrared spectroscopy concentration calculations for focal changes in oxygenation parameters," *Neuroimage* **18**(4), 865–879 (2003).
31. T. Durduran, "Non-invasive measurements of tissue hemodynamics with hybrid diffuse optical methods," Ph.D. Thesis, University of Pennsylvania, Philadelphia (2004).
32. X. Intes et al., "Diffuse optical tomography with physiological and spatial a priori constraints," *Phys. Med. Biol.* **49**(12), N155–N163 (2004).
33. M. Ferrari, M. Muthalib, and V. Quaresima, "The use of near-infrared spectroscopy in understanding skeletal muscle physiology: recent developments," *Philos. Trans. R. Soc. A* **369**(1955), 4577–4590 (2011).
34. G. Yu, "Near-infrared diffuse correlation spectroscopy in cancer diagnosis and therapy monitoring," *J. Biomed. Opt.* **17**(1), 010901 (2012)
35. E. M. Buckley et al., "Cerebral hemodynamics in preterm infants during positional intervention measured with diffuse correlation spectroscopy and transcranial Doppler ultrasound," *Opt. Express* **17**(15), 12571–12581 (2009).
36. R. Cheng et al., "Noninvasive optical evaluation of spontaneous low frequency oscillations in cerebral hemodynamics," *Neuroimage* **62**(3), 1445–1454 (2012).
37. L. Dong et al., "Noninvasive diffuse optical monitoring of head and neck tumor blood flow and oxygenation during radiation delivery," *Biomed. Opt. Express* **3**(2), 259–272 (2012).
38. T. Durduran et al., "Diffuse optical measurement of blood flow, blood oxygenation, and metabolism in a human brain during sensorimotor cortex activation," *Opt. Lett.* **29**(15), 1766–1768 (2004).
39. M. N. Kim et al., "Noninvasive measurement of cerebral blood flow and blood oxygenation using near-infrared and diffuse correlation spectroscopies in critically brain-injured adults," *Neurocrit. Care* **12**(2), 173–180 (2010).
40. N. Roche-Labarbe et al., "Noninvasive optical measures of CBV, StO (2), CBF index, and rCMRO(2) in human premature neonates' brains in the first six weeks of life," *Hum. Brain Mapp.* **31**(3), 341–352 (2010).
41. Y. Shang et al., "Diffuse optical monitoring of repeated cerebral ischemia in mice," *Opt. Express* **19**(21), 20301–20315 (2011).
42. Y. Shang et al., "Cerebral monitoring during carotid endarterectomy using near-infrared diffuse optical spectroscopies and electroencephalogram," *Phys. Med. Biol.* **56**(10), 3015–3032 (2011).
43. G. Yu et al., "Noninvasive monitoring of murine tumor blood flow during and after photodynamic therapy provides early assessment of therapeutic efficacy," *Clin. Cancer Res.* **11**(9), 3543–3552 (2005).
44. C. Zhou et al., "Diffuse optical monitoring of hemodynamic changes in piglet brain with closed head injury," *J. Biomed. Opt.* **14**(3), 034015 (2009).
45. Y. Shang et al., "Effects of muscle fiber motion on diffuse correlation spectroscopy blood flow measurements during exercise," *Biomed. Opt. Express* **1**(2), 500–511 (2010).
46. Y. Shang et al., "Portable optical tissue flow oximeter based on diffuse correlation spectroscopy," *Opt. Lett.* **34**(22), 3556–3558 (2009).

47. G. Yu et al., "Time-dependent blood flow and oxygenation in human skeletal muscles measured with noninvasive near-infrared diffuse optical spectroscopies," *J. Biomed. Opt.* **10**(2), 024027 (2005).
48. G. Yu et al., "Intraoperative evaluation of revascularization effect on ischemic muscle hemodynamics using near-infrared diffuse optical spectroscopies," *J. Biomed. Opt.* **16**(2), 027004 (2011).
49. K. Gurley, Y. Shang, and G. Yu, "Noninvasive optical quantification of absolute blood flow, blood oxygenation, and oxygen consumption rate in exercising skeletal muscle," *J. Biomed. Opt.* **17**(7), 075010 (2012).
50. L. He et al., "Using optical fibers with different modes to improve the signal-to-noise ratio of diffuse correlation spectroscopy flow-oximeter measurements," *J. Biomed. Opt.* **18**(3), 037001 (2013).
51. T. Li et al., "Simultaneous measurement of deep tissue blood flow and oxygenation using noncontact diffuse correlation spectroscopy flow-oximeter," *Sci. Rep.* **3**, 1358 (2013).
52. N. Munk et al., "Noninvasively measuring the hemodynamic effects of massage on skeletal muscle: a novel hybrid near-infrared diffuse optical instrument," *J. Bodyw. Mov. Ther.* **16**(1), 22–28 (2012).
53. Y. Shang et al., "Noninvasive optical characterization of muscle blood flow, oxygenation, and metabolism in women with fibromyalgia," *Arthritis Res. Ther.* **14**(6), R236 (2012).
54. G. Yu et al., "Validation of diffuse correlation spectroscopy for muscle blood flow with concurrent arterial spin labeled perfusion MRI," *Opt. Express* **15**(3), 1064–1075 (2007).
55. M. Belau et al., "Noninvasive observation of skeletal muscle contraction using near-infrared time-resolved reflectance and diffusing-wave spectroscopy," *J. Biomed. Opt.* **15**(5), 057007 (2010).
56. J. Dong et al., "Diffuse correlation spectroscopy with a fast Fourier transform-based software autocorrelator," *J. Biomed. Opt.* **17**(9), 097004 (2012).
57. D. A. Boas, L. E. Campbell, and A. G. Yodh, "Scattering and imaging with diffusing temporal field correlations," *Phys. Rev. Lett.* **75**(9), 1855–1858 (1995).
58. D. A. Boas and A. G. Yodh, "Spatially varying dynamical properties of turbid media probed with diffusing temporal light correlation," *J. Opt. Soc. Am. A-Opt. Image. Sci. Vis.* **14**(1), 192–215 (1997).
59. Y. L. Song et al., "Investigation of rat breast tumour oxygen consumption by hear-infrared spectroscopy," *J. Phys. D-Appl. Phys.* **38**(15), 2682–2690 (2005).
60. A. Duncan et al., "Optical pathlength measurements on adult head, calf and forearm and the head of the newborn infant using phase resolved optical spectroscopy," *Phys. Med. Biol.* **40**(2), 295–304 (1995).
61. P. Cosmo et al., "Effects of transcutaneous nerve stimulation on the microcirculation in chronic leg ulcers," *Scand. J. Plast. Reconstr. Surg. Hand Surg.* **34**(1), 61–64 (2000).
62. W. Phillips et al., "Relative changes in blood-flow with functional electrical-stimulation during exercise of the paralyzed lower-limbs," *Paraplegia* **33**(2), 90–93 (1995).
63. M. R. Roos et al., "Quadriceps muscle strength, contractile properties, and motor unit firing rates in young and old men," *Muscle Nerve* **22**(8), 1094–1103 (1999).
64. D. P. Currier, C. R. Petrilli, and A. J. Threlkeld, "Effect of graded electrical-stimulation on blood-flow to healthy muscle," *Phys. Ther.* **66**(6), 937–943 (1986).
65. R. C. Mesquita et al., "Diffuse optical characterization of an exercising patient group with peripheral artery disease," *J. Biomed. Opt.* **18**(5), 057007 (2013).
66. B. L. Edlow et al., "The effects of healthy aging on cerebral hemodynamic responses to posture change," *Physiol. Meas.* **31**(4), 477–495 (2010).
67. C. R. Bagshaw, *Muscle Contraction*, Chapman and Hall, London & New York (1982).
68. C. A. Phillips et al., "Biomimetic model of skeletal muscle isometric contraction: I. an energetic-viscoelastic model for the skeletal muscle isometric force twitch," *Comput. Biol. Med.* **34**(4), 307–322 (2004).
69. J. Bobet and R. B. Stein, "A simple model of force generation by skeletal muscle during dynamic isometric contractions," *IEEE Trans. Biomed. Eng.* **45**(8), 1010–1016 (1998).
70. A. M. King, D. S. Loiselle, and P. Kohl, "Force generation for locomotion of vertebrates: skeletal muscle overview," *IEEE J. Ocean. Eng.* **29**(3), 684–691 (2004).
71. M. C. P. van Beekvelt et al., "Performance of near-infrared spectroscopy in measuring local O-2 consumption and blood flow in skeletal muscle," *J. Appl. Physiol.* **90**(2), 511–519 (2001).